RESEARCH BRIEF

NRG1 Fusions in *KRAS* Wild-Type Pancreatic Cancer

Christoph Heining[1,2,3,4], Peter Horak[5,6,7], Sebastian Uhrig[7,8,9], Paula L. Codo[3,10], Barbara Klink[3,4,11,12], Barbara Hutter[7,8], Martina Fröhlich[7,8], David Bonekamp[13], Daniela Richter[1,3,4], Katja Steiger[14,15], Roland Penzel[7,16], Volker Endris[7,16], Karl Roland Ehrenberg[10,17], Stephanie Frank[10], Kortine Kleinheinz[18,19], Umut H. Toprak[9,18,20], Matthias Schlesner[20], Ranadip Mandal[21], Lothar Schulz[22], Helmut Lambertz[22], Sebastian Fetscher[23], Michael Bitzer[24,25], Nisar P. Malek[24,25], Marius Horger[25,26], Nathalia A. Giese[27], Oliver Strobel[27], Thilo Hackert[27], Christoph Springfeld[17], Lars Feuerbach[7,8], Frank Bergmann[16], Evelin Schröck[3,4,11,12], Christof von Kalle[5,6,7,28], Wilko Weichert[14,15], Claudia Scholl[7,21], Claudia R. Ball[1,3], Albrecht Stenzinger[7,16], Benedikt Brors[7,8], Stefan Fröhling[5,6,7,17], and Hanno Glimm[1,2,3,4]

ABSTRACT

We used whole-genome and transcriptome sequencing to identify clinically actionable genomic alterations in young adults with pancreatic ductal adenocarcinoma (PDAC). Molecular characterization of 17 patients with PDAC enrolled in a precision oncology program revealed gene fusions amenable to pharmacologic inhibition by small-molecule tyrosine kinase inhibitors in all patients with *KRAS* wild-type (*KRAS*^{WT}) tumors (4 of 17). These alterations included recurrent *NRG1* rearrangements predicted to drive PDAC development through aberrant ERBB receptor–mediated signaling, and pharmacologic ERBB inhibition resulted in clinical improvement and remission of liver metastases in 2 patients with *NRG1*-rearranged tumors that had proved resistant to standard treatment. Our findings demonstrate that systematic screening of *KRAS*^{WT} tumors for oncogenic fusion genes will substantially improve the therapeutic prospects for a sizeable fraction of patients with PDAC.

SIGNIFICANCE: Advanced PDAC is a malignancy with few treatment options that lacks molecular mechanism-based therapies. Our study uncovers recurrent gene rearrangements such as *NRG1* fusions as disease-driving events in *KRAS*^{WT} tumors, thereby providing novel insights into oncogenic signaling and new therapeutic options in this entity. *Cancer Discov; 8(9); 1087–95. ©2018 AACR.*

[1]Department of Translational Medical Oncology, National Center for Tumor Diseases (NCT) Dresden, Dresden, Germany. [2]University Hospital Carl Gustav Carus, Technische Universität Dresden, Dresden, Germany. [3]German Cancer Research Center (DKFZ), Heidelberg, Germany. [4]German Cancer Consortium (DKTK), Dresden, Germany. [5]Department of Translational Oncology, National Center for Tumor Diseases (NCT) Heidelberg and DKFZ, Heidelberg, Germany. [6]Section for Personalized Oncology, Heidelberg University Hospital, Heidelberg, Germany. [7]DKTK, Heidelberg, Germany. [8]Division of Applied Bioinformatics, DKFZ and NCT Heidelberg, Heidelberg, Germany. [9]Faculty of Biosciences, Heidelberg University, Heidelberg, Germany. [10]Translational Medical Oncology, National Center for Tumor Diseases (NCT) Heidelberg, Heidelberg, Germany. [11]Institute for Clinical Genetics, Faculty of Medicine Carl Gustav Carus, Technische Universität Dresden, Dresden, Germany. [12]National Center for Tumor Diseases (NCT) Dresden, Dresden, Germany. [13]Division of Radiology, DKFZ, Heidelberg, Germany. [14]Institute of Pathology, Technical University Munich, Munich, Germany. [15]DKTK, Munich, Germany. [16]Institute of Pathology, Heidelberg University Hospital, Heidelberg, Germany. [17]Department of Medical Oncology, NCT, Heidelberg, Germany. [18]Division of Theoretical Bioinformatics, DKFZ, Heidelberg, Germany. [19]Department for Bioinformatics and Functional Genomics, Institute for Pharmacy and Molecular Biotechnology and BioQuant, Heidelberg University, Heidelberg, Germany. [20]Bioinformatics and Omics Data Analytics, DKFZ, Heidelberg, Germany. [21]Division of Applied Functional Genomics, DKFZ, Heidelberg, Germany. [22]Department of Oncology, Klinikum Garmisch-Partenkirchen, Garmisch-Partenkirchen, Germany. [23]Department of Oncology, Sana Kliniken Lübeck, Lübeck, Germany. [24]Department of Gastroenterology, Hepatology and Infectious Diseases, Tübingen University Hospital, Tübingen, Germany. [25]DKTK, Tübingen, Germany. [26]Department of Radiology, Tübingen University Hospital, Tübingen, Germany. [27]Department of Surgery, Heidelberg University Hospital, Heidelberg, Germany. [28]DKFZ-Heidelberg Center for Personalized Oncology (HIPO), Heidelberg, Germany.

Note: Supplementary data for this article are available at Cancer Discovery Online (http://cancerdiscovery.aacrjournals.org/).

C. Heining, P. Horak, and S. Uhrig share first authorship of this article.

S. Fröhling and H. Glimm share last authorship of this article.

Corresponding Authors: Hanno Glimm, National Center for Tumor Diseases (NCT) Dresden and German Cancer Research Center (DKFZ) Heidelberg, 01309 Dresden, Germany. Phone: 49-351-458-5540; E-mail: hanno.glimm@nct-dresden.de; and Stefan Fröhling, National Center for Tumor Diseases (NCT) and German Cancer Research Center (DKFZ) Heidelberg, Im Neuenheimer Feld 460, 69120 Heidelberg, Germany. Phone: 49-6221-42-1634; Fax: 49-6221-42-1610; E-mail: stefan.froehling@nct-heidelberg.de

doi: 10.1158/2159-8290.CD-18-0036

INTRODUCTION

Pancreatic ductal adenocarcinoma (PDAC) is a major cause of cancer-related mortality and is projected to become the second leading cause of cancer-related death in 2030 (1). Treatment options for advanced PDAC are limited to few chemotherapy regimens and result in a median overall survival of less than 1 year (2, 3). Despite extensive efforts to molecularly characterize PDAC (4), a definition of therapeutically relevant subgroups based on somatic genetic alterations is missing, and stratified therapy is not established. More than 90% of PDAC cases harbor activating *KRAS* mutations that cannot be addressed therapeutically. Analysis of *KRAS* wild-type (*KRAS*^{WT}) tumors has revealed considerable genetic heterogeneity, including alterations of *GNAS, BRAF, CTNNB1*, and additional RAS pathway genes as potential oncogenic drivers (5); however, the clinical relevance of these alterations remains unclear, and none of them represent an established therapeutic target in this entity. The incidence of PDAC is strongly age related, with highest frequencies in patients ages 65 years and older, and available genomic data mirror this natural distribution. To address the unmet therapeutic need and understand the genetic landscape of PDAC in younger patients, we performed whole-exome/genome and transcriptome sequencing in a cohort of young patients enrolled in a genomics-guided precision oncology program.

RESULTS

Patient Cohort and Molecular Characteristics

Seventeen patients ages 24 to 49 years who had been diagnosed with PDAC (Table 1) were included in the National Center for Tumor Diseases/German Cancer Consortium (NCT/DKTK) Molecularly Aided Stratification for Tumor Eradication Research (MASTER) precision oncology program (6). Whole-exome sequencing (WES) and whole-genome sequencing (WGS) of tumor tissue identified 2 to 68 (average, 35.8) and 21 to 36 (average, 27.6) nonsynonymous point mutations, respectively. Small insertions/deletions (indels) in coding regions occurred with a maximum of five events per sample (average, 1.6). The number of somatic DNA copy-number aberrations ranged from 2 to 491 (WES, 2–97; WGS, 137–491). In total, 815 (WES, 275; WGS, 540) copy-number aberrations were broad events; 1,210 were focal with a size of 1 million base pairs (Mbp) or less (WES, 120; WGS, 1090). Most tumors harbored losses with regard to baseline ploidy (WES, 217 deletions and 178 gains; WGS, 999 deletions and 631 gains), including 158 homozygous events (WES, 49; WGS, 109). The majority of copy-number gains added a single copy. In 4 of 17 tumors, one or more high-level amplifications ($\log_2$ coverage ratio > 1.0) were observed. There were 4 to 151 [WES, 4–41 (average, 12); WGS, 44–151 (average, 75.2)] somatic structural variants supported by split reads in the DNA-sequencing data and 4 to 56 predicted gene fusions with medium or high confidence in the RNA-sequencing data (average, 21.5). The majority of samples (13 of 17, 76.5%) harbored *KRAS* p.G12D/R/V mutations, and most of these tumors displayed point mutations in *TP53* and loss of *CDKN2A/B* via focal deletions on chromosome 9p. In contrast, 4 of 17 tumors (23.5%) exhibited *KRAS*^{WT} and also lacked *TP53* alterations (Fig. 1; Supplementary Table S1). Analysis of germline data identified pathogenic variants in DNA repair genes in 3 of the 17 patients (17.6%), including two inactivating mutations in established PDAC predisposition genes (*PALB2* p.R170fsI*14 in patient 11 and *ATM* p.K1400* in patient 17). In patient 3, we detected a pathogenic *BLM* p.Y551* mutation in the germline that coincided with a somatic *BLM* p.D161N allele. In 5 additional patients, we found germline variants of uncertain significance (class 3 according to the American College of Medical Genetics and Genomics classification system) in genes involved in DNA repair, including an in-frame deletion in *NBN* as well as missense variants in *MSH2, PALLD, RAD50, FANCI*, and *WRN*.

Table 1. Patient characteristics and molecular analyses of patients with PDAC included in the NCT/DKTK MASTER precision oncology program

Patient characteristics	
Patients (*n*)	17
Age at the time of diagnosis (median, range)	39 (24–49)
Sex (*KRAS*-mutated tumors/*KRAS*^{WT} tumors)	
Male	12 (10/2)
Female	5 (3/2)
Systemic therapies prior to inclusion (median, range)	1 (0–3)
FOLFIRINOX	14
Gemcitabine and nab-paclitaxel	8
Other	2
Molecular analysis	
WES	12
WGS	5
Transcriptome sequencing	15

Oncogenic Gene Fusions in *KRAS* Wild-Type PDAC

We next performed a detailed analysis of structural genomic variations, including DNA copy-number changes and chromosomal rearrangements (Fig. 2A; Supplementary Fig. S1), and identified oncogenic gene fusions in all 4 *KRAS*^{WT} patients, whereas *KRAS*-mutated tumors lacked these rearrangements.

Three patients harbored complex structural rearrangements that relocated parts of *NRG1*, encoding a membrane-resident ligand for the ERBB3 pseudokinase, between two fusion partners that included *APP, CDH6, SARAF,* and *ATP1B1*. In each case, we identified two breakpoints within *NRG1*, yielding chimeric transcripts with truncated *NRG1* flanked by its 5′ and 3′ fusion partners. In patient 14, RNA sequencing revealed two transcript variants that differed by an attached intergenic sequence at the 3′ end of the fusion transcript. The EGF-like domain of *NRG1* was always retained in the chimeric transcript (Fig. 2B), whereas the *NRG1* transmembrane domains (TMn and TMc) were replaced by transmembrane domains provided by the respective fusion partner, analogous to previously described *CD74–NRG1* fusions (7). In all cases, the EGF-like domain of *NRG1* was predicted to reside in the extracellular space

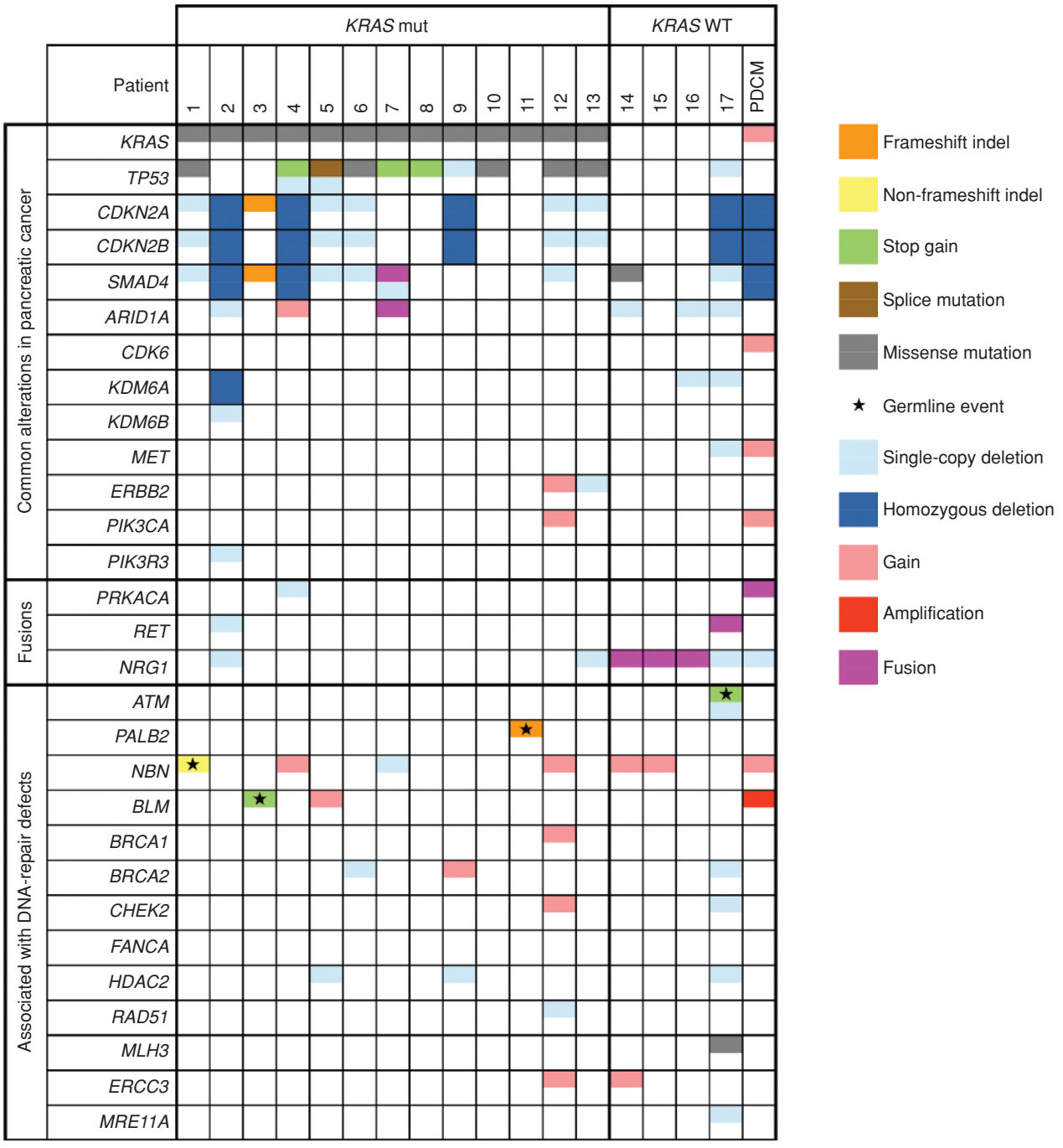

Figure 1. Molecular alterations in *KRAS*-mutant and *KRAS*^{WT} patients with PDAC and a *KRAS*^{WT} PDAC patient–derived cell model (PDCM). Activating *KRAS* mutations and oncogenic gene fusions were mutually exclusive. Inactivating *TP53* mutations frequently coincided with *KRAS* mutations, but were absent in *KRAS*^{WT} tumors. Table cells that are half-colored indicate hits of only a single allele. Fully colored table cells indicate biallelic hits. Sequencing coverage metrics are shown in Supplementary Table S2.

and interact with its receptors. In cases where transcriptome sequencing data were available, the splice patterns and exon coverage profiles indicated that the β transcript variant of *NRG1*, which has been shown to encode a protein with higher affinity to ERBB3/4 receptors (8), was expressed at higher levels than the α variant (Fig. 2C). In patient 14, *ATP1B1* constituted the 5′ end of the chimeric transcript and was fused to exons 2 to 7 of *NRG1*, which encode the immunoglobulin-like and EGF-like domains. The 3′ end of *NRG1* was truncated by means of a 10-Mbp deletion eliminating all exons following exon 7. The exon coverage profile revealed two transcript variants (Fig. 2B and D): a predominantly expressed short variant comprising the β and 3* exons of *NRG1*, and a minor variant that skipped the stop

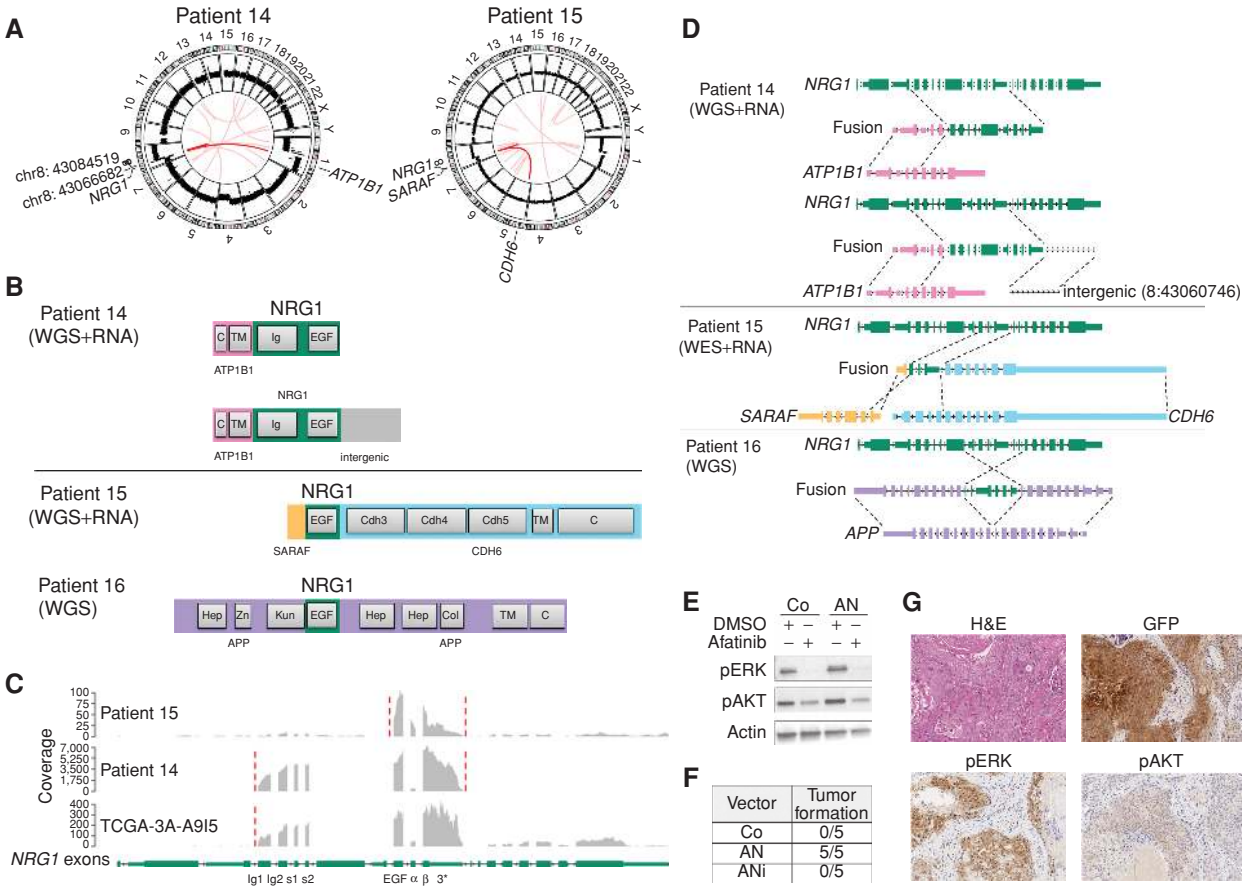

Figure 2. *NRG1* fusions. **A,** Circos plots of patients 14 and 15 showing DNA copy-number profiles and gene fusions predicted from transcriptome sequencing data. **B,** Protein domains predicted to be retained in the chimeric proteins. TM, transmembrane; C, cytoplasmic; EGF, epidermal growth factor-like; Ig, immunoglobulin-like; Hep, heparin-binding; Zn, zinc-binding; Kun, Kunitz; Col, collagen-binding; Cdh, cadherin. **C,** Coverage of *NRG1* exons in transcriptome sequencing data. Fusion breakpoints are indicated by red dashed lines. **D,** Fusion partners and retained exons. **E,** H6c7 cells transduced to stably express either GFP only (Co) or ATP1B1–NRG1 fusion including (ANi) or lacking (AN) the intergenic sequence. Western blotting demonstrated afatinib-sensitive AKT and ERK phosphorylation in H6c7 cells transduced with the AN fusion. **F,** *In vivo* transformation assays demonstrated tumor formation after 17 weeks in NSG mice transplanted with AN-transduced cells, but not Co- or ANi-transduced mice. **G,** IHC of an AN-induced xenograft tumor revealed constitutive ERK and AKT phosphorylation. H&E, hematoxylin and eosin.

codon in the 3* exon and contained a stretch of intergenic sequence with a 329-bp open reading frame. Overexpression of ATP1B1–NRG1 in H6c7 immortalized human pancreatic epithelial cells led to increased proliferation (Supplementary Fig. S2A and S2B) and enhanced AKT and ERK phosphorylation, which was abrogated upon treatment with the pan-ERBB inhibitor afatinib (Fig. 2E). Furthermore, H6c7 cells expressing ATP1B1–NRG1, but not cells transduced with the control vector or the fusion with attached intergenic region, formed tumors in immunocompromised mice with 100% penetrance (Fig. 2F and G).

In patient 15, the first exon of *SARAF* formed the 3′ end of the chimeric transcript and was juxtaposed to exons 6 to 7 of *NRG1*, which were fused to *CDH6* (Fig. 2D). In this transcript, NRG1 was predicted to be placed in the extracellular portion of CDH6, which contains a transmembrane domain that likely anchors the chimeric protein in the plasma membrane. In patient 16, the fusion transcript comprised *NRG1* exons 6 to 8 encoding the EGF-like domain. Both breakpoints linked *NRG1* to the *APP* gene, and the corresponding breakpoints in APP suggested that the EGF-like domain was embedded in the extracellular domain of APP (Fig. 2D). In patient 17, a balanced rearrangement described previously in non–small cell lung cancer (NSCLC) juxtaposed exons 1 to 9 of *NCOA4* to exons 12 to 20 of *RET* encoding the RET kinase domain (Supplementary Fig. S3A; ref. 9).

To corroborate that oncogenic gene fusions are common events in $KRAS^{WT}$ PDAC, we assessed the *KRAS* mutation status of 17 primary cell cultures derived from patients with PDAC across age groups and identified one $KRAS^{WT}$ tumor. Transcriptome sequencing detected a highly expressed fusion transcript involving the 5′ end of *ATP1B1* fused to exon 2 of *PRKACA* (Supplementary Fig. S3B). In addition, we queried the publicly available PDAC dataset from The Cancer Genome Atlas (TCGA) and identified 1 $KRAS^{WT}$ patient (TCGA-3A-A9I5) with an *ATP1B1–NRG1* fusion (Supplementary Fig. S3C) similar to the one observed in patient 14. The exon coverage profile of *NRG1* suggested that the predominant transcript was the same as in patient 14.

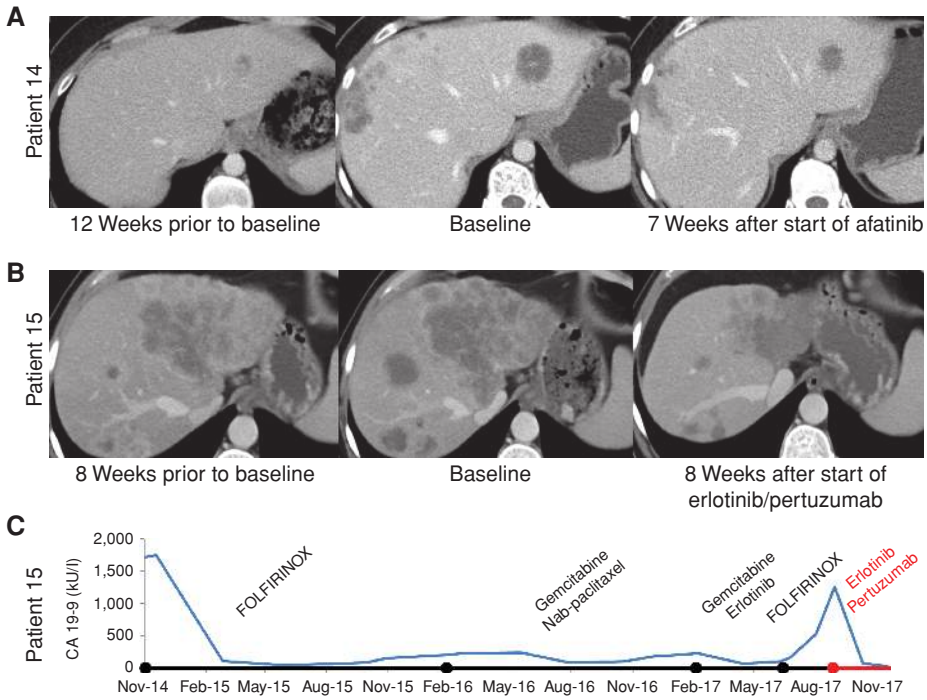

Figure 3. Response to targeted therapy in 2 patients with PDAC harboring *NRG1* fusions. **A,** CT scans showing tumor growth prior to afatinib therapy and response of liver metastases to afatinib after 7 weeks of treatment in patient 14. Baseline CT scans were taken before the start of afatinib therapy. **B,** CT scans showing initial growth during FOLFIRINOX treatment and response of liver metastases to erlotinib/pertuzumab combination therapy after 8 weeks in patient 15. **C,** Time course of serum CA 19-9 levels in patient 15 showing initial response to FOLFIRINOX and disease stabilization under subsequent therapies as well as rapid progression during retreatment with FOLFIRINOX. Decline of serum CA 19-9 levels to normal values was observed with erlotinib/pertuzumab therapy (indicated in red).

Clinical Course and Treatment of Patients with KRAS Wild-Type, NRG1-Rearranged PDAC

Two of the 3 patients with *KRAS*^{WT}, *NRG*-rearranged PDAC were treated in accordance with the recommendations by the NCT/DKTK MASTER molecular tumor board. The clinical course of the third patient is summarized in the Supplementary Data.

Patient 14, a 30-year-old female, was diagnosed with poorly differentiated, metastatic PDAC at the age of 29. First-line therapy with FOLFIRINOX (2) for 7 months resulted in stable disease as best response. Following progression, monotherapy with afatinib, an orally available pan-ERBB inhibitor, was started based on our molecular and functional studies, which suggested that this patient's tumor was driven by aberrant ERBB signaling mediated by the ATP1B1–NRG1 fusion. A CT scan 7 weeks after initiation of therapy demonstrated a substantial decrease in size and contrast medium enhancement of liver metastases (Fig. 3A). During afatinib therapy, cutaneous side effects required intermittent dose reduction. A second follow-up CT scan 3 months later revealed tumor progression.

Patient 15, a 42-year-old female, had been diagnosed with metastatic PDAC at the age of 39. First-line chemotherapy with FOLFIRINOX resulted in disease stabilization for 15 months. Following progression, therapy was switched to gemcitabine and nab-paclitaxel, which led to disease control for another 9 months. Third-line therapy consisted of gemcitabine and erlotinib, an oral selective EGFR tyrosine kinase inhibitor, and was administered until progression 5 months later. Three cycles of FOLFIRINOX salvage therapy could not halt further progression of liver metastases. Based on the tumor's molecular profile, combination therapy with erlotinib and pertuzumab, a humanized monoclonal antibody preventing dimerization of ERBB2 with other ERBB receptors, was started. Reevaluation after 8 weeks showed a partial remission of liver metastases and normalization of serum CA19-9 levels (Fig. 3B and C). Restaging 3 months later showed radiographic disease progression despite CA19-9 levels within normal range.

DISCUSSION

This comprehensive molecular analysis of PDAC, a clinically challenging entity commonly viewed as "undruggable," in a cohort of young adults has revealed a high incidence of immediately targetable genetic alterations. Specifically, we identified gene fusions involving *NRG1* or *RET*, which are amenable to pharmacologic inhibition using small-molecule tyrosine kinase inhibitors, in all patients with *KRAS*^{WT} tumors. The consistent finding of fusion genes predicted to result in constitutive receptor tyrosine kinase activity suggests that such rearrangements represent driving genomic events in the absence of oncogenic KRAS signaling, a notion that is also supported by the mutual exclusivity of *KRAS* mutations and *NRG1* rearrangements in lung adenocarcinoma (7). *NCOA4–RET* fusions similar to the one observed in one of our patients have been described previously in papillary thyroid carcinoma and lung adenocarcinoma (9). *In silico* analysis of publicly available TCGA data and functional studies in patient-derived PDAC models uncovered one additional *NRG1* fusion as well as a novel, putatively oncogenic *PRKACA* fusion. In both cases, age at diagnosis was well above 50 years, supporting the relevance of our findings in a larger proportion of patients with PDAC.

NRG1 is a ligand of the ERBB3 and ERBB4 receptors (10, 11), and recruitment of EGFR and/or ERBB2 by activated ERBB3/4 leads to stimulation of downstream signaling pathways. The detection of *NRG1* fusions in young patients with PDAC, some of whom experienced comparatively slow disease progression, hints at a distinct pathogenesis in a subset

of patients with PDAC. The CD74–NRG1 fusion acts as an oncogenic driver in the mucinous subtype of lung adenocarcinoma (7). Mechanistically, CD74–NRG1 leads to enhanced expression of the EGF-like domain of NRG1, which serves as ligand for ERBB2/ERBB3 receptor complexes (12) and provides a rationale for ERBB-targeted therapies. Several clinical trials in unselected patients with PDAC failed to show efficacy of ERBB inhibition, and the approval of the tyrosine kinase inhibitor erlotinib in this entity is based on a modest overall survival benefit (13–15). However, in one phase II trial, significant clinical efficacy of nimotuzumab, an anti-EGFR antibody, in combination with gemcitabine was evident in *KRAS*^{WT} patients (16), and a retrospective analysis of the AIO-PK0104 trial demonstrated improved survival of *KRAS*^{WT} patients treated with erlotinib (17), although no predictive value could be assigned to the KRAS status (18).

There are different options to target NRG1-driven ERBB signaling pharmacologically. NRG1-mediated secondary resistance to lapatinib or erlotinib in breast cancer models can be overcome by the addition of pertuzumab, an antibody that prevents ERBB2 interaction with other ERBB family members (19), or pan-ERBB inhibition with afatinib (20), respectively, and NRG1-mediated tumor growth can be successfully inhibited by pertuzumab (21). Recently, responses to afatinib were observed in 2 patients with *NRG1*-rearranged lung and cholangiocellular adenocarcinoma, respectively (22). Afatinib has also demonstrated preclinical activity in PDAC (23) and can be safely combined with taxanes. Another option is the combination of erlotinib and pertuzumab, a strategy that is therapeutically active in NSCLC (24). Both afatinib and erlotinib plus pertuzumab resulted in clinically relevant responses in patients with *NRG1*-rearranged PDAC identified in this study. Although our findings support expanding ERBB-directed inhibition toward all ERBB family members and their dimerization, side effects and clinical activity of different combination partners will need to be assessed to define the optimal treatment regimen in this setting.

Our analysis of germline data revealed a considerable number of rare variants in cancer-associated genes. Known pathogenic germline mutations in DNA repair genes were found in 3 of 17 patients and affected *PALB2, ATM*, and *BLM*. In addition, we identified variants of uncertain significance in several genes involved in DNA repair. Previous studies found germline mutations in *BRCA1, BRCA2*, and *PALB2* as well as in mismatch-repair genes in 10% to 15% of patients with PDAC. These mutations result in defects of homologous recombination (HR), thus sensitizing the tumor toward platinum-based therapy and PARP inhibitors (25). In our cohort, we observed a significant number of potentially clinically relevant germline alterations affecting HR, which are not evaluated routinely.

Collectively, our results indicate that *KRAS*^{WT} PDAC is driven by oncogenic gene fusions that can be targeted with clinically available drugs. In view of the structural complexity of *NRG1* rearrangements, we propose a two-tiered molecular diagnostic approach, including screening for *KRAS*^{WT} tumors and subsequent detection of clinically actionable gene fusions that will enable stratification and molecular mechanism-based treatment of patients with this intractable disease.

METHODS

Next-Generation Sequencing, Bioinformatic Analysis, and Target Validation

DNA from tumor tissue was isolated using the AllPrep DNA/RNA/miRNA Universal Kit (Qiagen), and peripheral blood was isolated using the QIAamp DNA Blood Mini Kit (Qiagen), followed by quality control using gel electrophoresis and a TapeStation 2200 system (Agilent). Samples were prepared either for WGS or WES. Exome capturing was performed using SureSelect Human All Exon V5 (+UTRs, if RNA was unavailable) in-solution capture reagents (Agilent). If samples were destined for WES on an Illumina HiSeq 2500 instrument, then 1.5 μg genomic DNA were fragmented to 150 to 200 bp insert size with a Covaris S2 device, and 250 ng of Illumina adapter-containing libraries were hybridized with exome baits at 65°C for 16 hours. If samples were destined for WES on an Illumina HiSeq 4000 instrument, then 200 ng genomic DNA was fragmented to 300 bp insert size with a Covaris LE220 or E220 device, and 750 ng of adapter-containing libraries were hybridized with exome baits at 65°C for 16 hours. If samples were destined for WGS on an Illumina HiSeq X instrument, then 100 ng of genomic DNA were fragmented to 450 bp insert size with a Covaris LE220 or E220 device, and libraries were prepared using the TruSeq Nano Kit (Illumina). On all platforms paired-end sequencing was carried out according to the manufacturer's recommendations, yielding read lengths of 101 bp (HiSeq 2500 and 4000) or 151 bp (HiSeq X). RNA-sequencing libraries were prepared using the TruSeq RNA Sample Preparation Kit v2 (Illumina). Briefly, mRNA was purified from 1 μg total RNA using oligo(dT) beads, poly(A)$^+$ RNA was fragmented to 150 bp and converted into cDNA, and cDNA fragments were end-repaired, adenylated on the 3′ end, adapter-ligated, and amplified with 12 cycles of polymerase chain reaction. The final libraries were validated using a Qubit 2.0 Fluorometer (Life Technologies) and a Bioanalyzer 2100 system (Agilent). Libraries were sequenced on an Illumina-patterned flowcell v2.5.

Reads were mapped to the 1000 Genomes Phase II assembly of the human reference genome (NCBI build 37.1). Genome sequencing data generated on the HiSeq 2500 platform were aligned using the *aln* module of BWA (version 0.6.2) with default parameters and maximum insert size set to 1,000 bp (26); genome-sequencing data generated on the HiSeq 4000 and X platforms were aligned using the *mem* module of BWA (version 0.7.15) with default parameters and filtering by alignment score disabled. BAM files were sorted with SAMtools (version 0.1.19; ref. 27), and duplicates were marked with Picard tools (version 1.125). Single-nucleotide variants (SNV) and small insertions/deletions (indels) were analyzed using a previously reported bioinformatics workflow (28). Copy-number variants (CNV) were extracted from the WES samples with the help of CNVkit (version 0.8.3.dev0; ref. 29). For the extraction of CNVs from WGS data, we used our in-house CNV calling pipeline ACEseq (allele-specific copy-number estimation from WGS). ACEseq determines absolute allele-specific copy numbers as well as tumor ploidy and tumor cell content based on coverage ratios of tumor and control as well as the B-allele frequency (BAF) of heterozygous SNPs. To improve genome segmentation, structural variants called by our in-house pipeline SOPHIA (v34.1, default parameters) were incorporated. Briefly, SOPHIA is based on supplementary alignments reported by the bwa-mem aligner. It uses a decision tree to designate high-quality reads and low-quality reads that fall on poorly mappable regions or appear due to low-quality base calls. The remaining high-quality reads are further filtered using a background population model trained on control (blood) sequencing data from 3,261 patients from published TCGA cohorts and published/unpublished DKFZ cohorts. A structural variant is discarded if: (i) the ratio of low-quality reads supporting one of the breakpoints exceeds 85%; (ii) the structural variant is detected on only one breakpoint (with the second either unmappable or undetected) and the exact same

breakpoint was detected in more than three cases in the 3,261 patient population background model; (iii) the structural variant is detected by two breakpoints and one of them was exactly detected in more than 3% of the 3,261 patient population background model; (iv) both of the detected breakpoints had less than 5% allele frequency. Structural variants were detected in WES data using CREST (30). All events were annotated with RefSeq genes using BEDTools (31).

RNA-sequencing data generated on the HiSeq 2500 platform were processed as described previously (28); RNA-sequencing data generated on the HiSeq 4000 platform were aligned using STAR 2.5.1b (32) with the same parameters as with STAR 2.3.0e and additionally chimSeqmentReadGapMax set to 3 and alignSJstitchMismatchNmax set to "5 −1 5 5." We extracted high-confidence gene fusion predictions from the chimeric alignments produced by STAR using our in-house pipeline Arriba, which removes recurrent alignment artifacts, transcript variants also observed in normal tissue, reads with low sequence complexity, and events with short anchors or breakpoints in close proximity or a low number of supporting reads relative to the overall number of predicted events in a gene.

Validation of clinically relevant aberrations was performed using Sanger sequencing. For patient 16, 1 μg RNA was used as a template for cDNA synthesis using the RevertAid First Strand cDNA synthesis kit (Life Technologies; K1622) according to the manufacturer's instructions. Primers were designed to align to the patient-specific *APP–NRG1* fusion breakpoints (Forward: CCGA GATCCTGTTAAACCTACA; Reverse: AGGAATGTAGAAGCTGGC CATT) and used for RT-PCR at the following conditions: initial denaturation: 120 seconds at 94°C; 30 cycles of extension: 30 seconds 94°C, 30 seconds 51°C, 45 seconds 72°C; final extension: 10 minutes at 72°C. Gel band at the expected size (211 bp) was cut, purified (Gel Extraction Kit, Qiagen), and validated by Sanger sequencing (GATC).

KRAS Mutation Analysis

PDAC patient-derived cultures were cultured as described (33) and harvested for mRNA extraction (RNAEasy Mini Kit, Qiagen) and cDNA synthesis (RevertAid First Strand cDNA Synthesis Kit, Life Technologies; K1622). *KRAS* Exon 2 was amplified by PCR using Phusion High-Fidelity PCR Kit (NEB) with the following primers: *KRAS* Forward: GCCATTTCGGACTGGGAGCGA; *KRAS* Reverse: GGCATCATCAACACCCAGATTAC. PCR program consisted of initial denaturation: 30 seconds at 98°C; 35 cycles of extension: 10 seconds 98°C, 30 seconds 60°C, 30 seconds 72°C; final extension: 7 minutes at 72°C. The PCR products were separated on a 1% agarose gel containing 0.05% ethydium bromide. Single bands at the expected MW (0.7 kb) were cut, purified (Gel Extraction Kit, Qiagen), and sent for Sanger sequencing (GATC) using the following primers: primer 1: CGGACTGGGAGCGAGCGC; primer 2: GCATCCTCCACTCTCT GTCTT.

Cell Growth Assay

Two versions of the *ATP1B1–NRG1* fusion sequence with and without the intergenic sequence (ANi and AN, respectively) found in patient 14 were synthesized (GeneScript) and cloned into the pCCL.SIN.cPPT.PGK.eGFP.wPRE lentiviral vector backbone, and lentiviral particles were produced as described (34). Immortalized human pancreatic duct epithelial cells H6c7 (Kerafast, ref. 35) were cultivated at 37°C, 5% CO_2 with keratinocyte medium (Gibco) supplemented with 5 μg/L of human epithelial growth factor (EGF; Gibco) and 50 mg/L of bovine pituitary extract (BPE; Gibco) and kept in an incubator at 37°C and 5% CO_2. H6c7 cells were transduced with empty vector (Co), ANi, and AN lentiviral constructs at multiplicities of infection 1 and 10 with polybrene (8 μg/mL, Millipore) for 24 hours. Transduction efficiency was confirmed after 5 days by FACS analysis, and cells were expanded and sorted for GFP expression. mRNA and cDNA from transduced cells were prepared as described above. Expression of the constructs was determined by qPCR according to the manufacturer's instructions (PowerSybr green, AB) using the following primers: Fusion product: Forward: ACATATCAGGAC CGAGTGGC, Reverse: CACTTGAATCTGAGAGAGGAG; Intergenic sequence: Forward: TACTGGTGATCGCTGCCAA, Reverse: CTGC CTGGTGACCCAT. Transforming capacity was measured as fold change of ATP content as surrogate of viable cells. In brief, H6C7 cells stably transduced with Co, ANi, or AN lentiviral vectors were seeded into 384-well plates at a density of 1,000 cells per well in 50 μL of Keratinocyte medium + EGF/BPE. ATP content was measured at days 0 and 7 using the ATPlite 1step luminescence kit (Perkin Elmer) at a plate reader (Tecan).

H6c7 cells were regularly tested for *Mycoplasma* contamination using the Venor GeM Mycoplasma Detection Kit (Minerva) before and after conducting experiments. Cells were thawed at early passage >4 weeks and cultured for up to 12 weeks in total.

Western Blotting

H6c7 cells transduced with control, ANinter, or AN lentiviral constructs were plated at a density of 5×10^5 cells per 6-cm dish and kept for 24 hours on medium without EGF and BPE. Sixty minutes prior to harvesting, cells were treated with 0.1% v/v DMSO (Sigma-Aldrich) or 10 μmol/L afatinib (Selleckchem).

Cells were scraped and lysed in ice-cold lysis buffer (Tris–HCl 20 mmol/L pH 7.5, NaCl 150 mmol/L, NaF 10 mmol/L, Triton X-100 1%). Protein concentration was determined using the Pierce BCA Protein assay kit (Thermo Fisher Scientific), and 15 μg of protein was loaded per line in MiniPROTEAN TGXTM PreCast gels (Bio-Rad) with appropriate amount of 4× Laemmli Sample Buffer (#161-07474x, Bio-Rad). Transfer was done using the Trans-Blot Turbo Mini PVDF Transfer Packs #1704156 for the Trans-Blot Turbo transfer system (Bio-Rad). The primary antibodies used were rabbit polyclonal #9275s Phospho-AKT (Thr308), rabbit mAb #4376 Phospho-p44/42 MAPK (ERK1/2; Thr202/Tyr204; 20G11; Cell Signaling Technology), and mouse mAb #A3853 Actin Sigma (Sigma-Aldrich). All primary antibodies were diluted 1/1,000 in TBS-T 5% BSA and incubated overnight at 4°C. The secondary antibodies Rabbit Anti-Mouse IgG H&L (HRP; ab6728) and Goat Anti-Rabbit IgG H&L (HRP; ab6721) from Abcam were used at 1/10,000 dilution in TBS-T 5% BSA, incubated 1 hour at room temperature. Membranes were developed using PierceTM ECL western blotting developing substrate (Thermo Fisher Scientific) and the ChemiDocTM Imaging System (Bio-Rad).

In Vivo *Transformation* Assay

Transduced cells (1×10^6) were mixed 1:1 with matrigel (BD Biosciences) and transplanted subcutaneously into NOD.Cg-Prkdc^{scid}Il2rg^{tm1Wjl}/SzJ (NSG) mice (five per construct; The Jackson Laboratory). Tumor size was measured weekly. At week 17, one xenograft tumor was harvested, fixed in 10% formalin, and submitted for IHC. All mouse experiments were performed according to the German Animal Protection laws and regulations approved by the ethical committee.

IHC

IHC was performed using a Bond RXm system (Leica) with primary antibodies against phospho-ERK1/2 (Cell Signaling Technology; #4376, 1:1,000) and phospho-AKT (Cell Signaling Technology; #4060, 1:50). Briefly, slides were deparaffinized, pretreated with Epitope Retrieval Solution 2 for 30 (phospho-ERK1/2) or 60 minutes (phospho-AKT), and incubated with the primary antibody for 15 minutes at room temperature (phospho-ERK1/2) or 30 minutes at 38°C (phospho-AKT). Antibody binding was detected with a polymer refine detection kit without post primary reagent and visualized with 3,3′-diaminobenzidine as dark brown precipitate. Counterstaining was performed with hematoxylin.

Accession Code

Sequencing data were deposited in the European Genome-phenome Archive under accession number EGAS00001002759.

Disclosure of Potential Conflicts of Interest

D. Bonekamp has received honoraria from the speakers' bureau of Profound Medical Inc. W. Weichert reports receiving a commercial research grant from Roche, has received honoraria from the speakers bureaus of Pfizer, Roche, MSD, BMS, AstraZeneca, and Novartis, and is a consultant/advisory board member for Pfizer, Roche, MSD, BMS, AstraZeneca, and Novartis. A. Stenzinger is a consultant/advisory board member for AstraZeneca, BMS, Novartis, and Roche. No potential conflicts of interest were disclosed by the other authors.

Authors' Contributions

Conception and design: C. Heining, P. Horak, R. Mandal, S. Fröhling, H. Glimm

Development of methodology: P.L. Codo, B. Hutter, R. Mandal, C.R. Ball, S. Fröhling

Acquisition of data (provided animals, acquired and managed patients, provided facilities, etc.): C. Heining, P. Horak, P.L. Codo, K. Steiger, R. Penzel, K.R. Ehrenberg, S. Frank, L. Schulz, H. Lambertz, S. Fetscher, M. Bitzer, N.P. Malek, M. Horger, N.A. Giese, O. Strobel, T. Hackert, C. Springfeld, F. Bergmann, C. von Kalle, W. Weichert, C. Scholl, C.R. Ball, A. Stenzinger, S. Fröhling, H. Glimm

Analysis and interpretation of data (e.g., statistical analysis, biostatistics, computational analysis): C. Heining, P. Horak, S. Uhrig, P.L. Codo, B. Klink, B. Hutter, M. Fröhlich, D. Bonekamp, K. Steiger, R. Penzel, V. Endris, K.R. Ehrenberg, K. Kleinheinz, U.H. Toprak, M. Schlesner, S. Fetscher, M. Bitzer, M. Horger, L. Feuerbach, F. Bergmann, E. Schröck, W. Weichert, C.R. Ball, A. Stenzinger, B. Brors, S. Fröhling, H. Glimm

Writing, review, and/or revision of the manuscript: C. Heining, P. Horak, S. Uhrig, P.L. Codo, B. Klink, D. Bonekamp, K. Kleinheinz, U.H. Toprak, M. Bitzer, M. Horger, O. Strobel, T. Hackert, C. Springfeld, L. Feuerbach, F. Bergmann, W. Weichert, C.R. Ball, A. Stenzinger, S. Fröhling, H. Glimm

Administrative, technical, or material support (i.e., reporting or organizing data, constructing databases): D. Richter, O. Strobel, T. Hackert, A. Stenzinger

Study supervision: M. Schlesner, T. Hackert, B. Brors, S. Fröhling, H. Glimm

Other (designed and performed *in vitro* and *in vivo* experiments): P.L. Codo

Other (image interpretation): M. Horger

Acknowledgments

The authors thank the DKFZ-HIPO Sample Processing Laboratory, the DKFZ Genomics and Proteomics Core Facility, and the DKFZ-HIPO Data Management Group for technical support. We also thank K. Beck, K. Willmund, R. Eils, and P. Lichter for infrastructure and program development within DKFZ-HIPO. Tissue samples were provided by the NCT and Pancobank/EPZ-Surgery Heidelberg Tissue Banks in accordance with Biomaterialbank Heidelberg regulations and after approval by the Ethics Committee of Heidelberg University. This work was supported by grant 021 from DKFZ-HIPO, the NCT 3.0 Precision Oncology Program (NCT POP), NCT 3.0 Section Personalized Medicine (NCT3.0_2015.4 TransOnco), and a grant from the NCT 3.0 Integrative Projects in Basic Cancer Research Program. P.L. Codo and S. Frank were supported by a postdoctoral fellowship and a Heinrich F.C. Behr stipend from the DKFZ, respectively. PancoBank/EPZ-Surgery was supported by BMBF grants 01ZX1305C/1605C, EU ERA-Net TRANSCAN01KT1506, and Heidelberger Stiftung Chirurgie.

The costs of publication of this article were defrayed in part by the payment of page charges. This article must therefore be hereby marked *advertisement* in accordance with 18 U.S.C. Section 1734 solely to indicate this fact.

Received January 11, 2018; revised April 24, 2018; accepted May 24, 2018; published first May 25, 2018.

REFERENCES

1. Rahib L, Smith BD, Aizenberg R, Rosenzweig AB, Fleshman JM, Matrisian LM. Projecting cancer incidence and deaths to 2030: the unexpected burden of thyroid, liver, and pancreas cancers in the United States. Cancer Res 2014;74:2913–21.
2. Conroy T, Desseigne F, Ychou M, Bouche O, Guimbaud R, Becouarn Y, et al. FOLFIRINOX versus gemcitabine for metastatic pancreatic cancer. N Engl J Med 2011;364:1817–25.
3. Von Hoff DD, Ervin T, Arena FP, Chiorean EG, Infante J, Moore M, et al. Increased survival in pancreatic cancer with nab-paclitaxel plus gemcitabine. N Engl J Med 2013;369:1691–703.
4. Bailey P, Chang DK, Nones K, Johns AL, Patch AM, Gingras MC, et al. Genomic analyses identify molecular subtypes of pancreatic cancer. Nature 2016;531:47–52.
5. Cancer Genome Atlas Research Network. Electronic address aadhe, cancer genome atlas research N. integrated genomic characterization of pancreatic ductal adenocarcinoma. Cancer Cell 2017;32:185–203 e13.
6. Horak P, Klink B, Heining C, Groschel S, Hutter B, Frohlich M, et al. Precision oncology based on omics data: the NCT Heidelberg experience. Int J Cancer. 2017.
7. Fernandez-Cuesta L, Plenker D, Osada H, Sun R, Menon R, Leenders F, et al. CD74–NRG1 fusions in lung adenocarcinoma. Cancer Discov 2014;4:415–22.
8. Tzahar E, Levkowitz G, Karunagaran D, Yi L, Peles E, Lavi S, et al. ErbB-3 and ErbB-4 function as the respective low and high affinity receptors of all Neu differentiation factor/heregulin isoforms. J Biol Chem 1994;269:25226–33.
9. Wang R, Hu H, Pan Y, Li Y, Ye T, Li C, et al. RET fusions define a unique molecular and clinicopathologic subtype of non–small-cell lung cancer. J Clin Oncol 2012;30:4352–9.
10. Ieguchi K, Fujita M, Ma Z, Davari P, Taniguchi Y, Sekiguchi K, et al. Direct binding of the EGF-like domain of neuregulin-1 to integrins ({alpha}v{beta}3 and {alpha}6{beta}4) is involved in neuregulin-1/ErbB signaling. J Biol Chem 2010;285:31388–98.
11. Sweeney C, Lai C, Riese DJ II, Diamonti AJ, Cantley LC, Carraway KL III. Ligand discrimination in signaling through an ErbB4 receptor homodimer. J Biol Chem 2000;275:19803–7.
12. Falls DL. Neuregulins: functions, forms, and signaling strategies. Exp Cell Res 2003;284:14–30.
13. Safran H, Iannitti D, Ramanathan R, Schwartz JD, Steinhoff M, Nauman C, et al. Herceptin and gemcitabine for metastatic pancreatic cancers that overexpress HER-2/neu. Cancer Invest 2004;22:706–12.
14. Safran H, Miner T, Bahary N, Whiting S, Lopez CD, Sun W, et al. Lapatinib and gemcitabine for metastatic pancreatic cancer. A phase II study. Am J Clin Oncol 2011;34:50–2.
15. Moore MJ, Goldstein D, Hamm J, Figer A, Hecht JR, Gallinger S, et al. Erlotinib plus gemcitabine compared with gemcitabine alone in patients with advanced pancreatic cancer: a phase III trial of the National Cancer Institute of Canada Clinical Trials Group. J Clin Oncol 2007;25:1960–6.
16. Schultheis B, Reuter D, Ebert MP, Siveke J, Kerkhoff A, Berdel WE, et al. Gemcitabine combined with the monoclonal antibody nimotuzumab is an active first-line regimen in KRAS wildtype patients with locally advanced or metastatic pancreatic cancer: a multicenter, randomized phase IIb study. Ann Oncol 2017;28:2429–35.
17. Boeck S, Jung A, Laubender RP, Neumann J, Egg R, Goritschan C, et al. EGFR pathway biomarkers in erlotinib-treated patients with advanced pancreatic cancer: translational results from the randomised, crossover phase 3 trial AIO-PK0104. Br J Cancer 2013;108:469–76.

18. Boeck S, Jung A, Laubender RP, Neumann J, Egg R, Goritschan C, et al. KRAS mutation status is not predictive for objective response to anti-EGFR treatment with erlotinib in patients with advanced pancreatic cancer. J Gastroenterol 2013;48:544–8.
19. Capelan M, Pugliano L, De Azambuja E, Bozovic I, Saini KS, Sotiriou C, et al. Pertuzumab: new hope for patients with HER2-positive breast cancer. Ann Oncol 2013;24:273–82.
20. Yonesaka K, Kudo K, Nishida S, Takahama T, Iwasa T, Yoshida T, et al. The pan-HER family tyrosine kinase inhibitor afatinib overcomes HER3 ligand heregulin-mediated resistance to EGFR inhibitors in non-small cell lung cancer. Oncotarget 2015;6:33602–11.
21. Leung WY, Roxanis I, Sheldon H, Buffa FM, Li JL, Harris AL, et al. Combining lapatinib and pertuzumab to overcome lapatinib resistance due to NRG1-mediated signalling in HER2-amplified breast cancer. Oncotarget 2015;6:5678–94.
22. Jones MR, Lim H, Shen Y, Pleasance E, Ch'ng C, Reisle C, et al. Successful targeting of the NRG1 pathway indicates novel treatment strategy for metastatic cancer. Ann Oncol 2017;28:3092–7.
23. Huguet F, Fernet M, Giocanti N, Favaudon V, Larsen AK. Afatinib, an irreversible EGFR family inhibitor, shows activity toward pancreatic cancer cells, alone and in combination with radiotherapy, independent of KRAS status. Target Oncol 2016;11:371–81.
24. Hughes B, Mileshkin L, Townley P, Gitlitz B, Eaton K, Mitchell P, et al. Pertuzumab and erlotinib in patients with relapsed non-small cell lung cancer: a phase II study using 18F-fluorodeoxyglucose positron emission tomography/computed tomography imaging. Oncologist 2014;19:175–6.
25. Kaufman B, Shapira-Frommer R, Schmutzler RK, Audeh MW, Friedlander M, Balmana J, et al. Olaparib monotherapy in patients with advanced cancer and a germline BRCA1/2 mutation. J Clin Oncol 2015;33:244–50.
26. Li H, Durbin R. Fast and accurate short read alignment with burrows-wheeler transform. Bioinformatics 2009;25:1754–60.
27. Li H, Handsaker B, Wysoker A, Fennell T, Ruan J, Homer N, et al. The sequence alignment/map format and SAMtools. Bioinformatics 2009;25:2078–9.
28. Kordes M, Roring M, Heining C, Braun S, Hutter B, Richter D, et al. Cooperation of BRAF(F595L) and mutant HRAS in histiocytic sarcoma provides new insights into oncogenic BRAF signaling. Leukemia 2016;30:937–46.
29. Talevich E, Shain AH, Botton T, Bastian BC. CNVkit: genome-wide copy number detection and visualization from targeted DNA sequencing. PLoS Comput Biol 2016;12:e1004873.
30. Wang J, Mullighan CG, Easton J, Roberts S, Heatley SL, Ma J, et al. CREST maps somatic structural variation in cancer genomes with base-pair resolution. Nat Methods 2011;8:652–4.
31. Quinlan AR, Hall IM. BEDTools: a flexible suite of utilities for comparing genomic features. Bioinformatics 2010;26:841–2.
32. Dobin A, Davis CA, Schlesinger F, Drenkow J, Zaleski C, Jha S, et al. STAR: ultrafast universal RNA-seq aligner. Bioinformatics 2013;29:15–21.
33. Ball CR, Oppel F, Ehrenberg KR, Dubash TD, Dieter SM, Hoffmann CM, et al. Succession of transiently active tumor-initiating cell clones in human pancreatic cancer xenografts. EMBO Mol Med 2017;9:918–32.
34. Follenzi A, Ailles LE, Bakovic S, Geuna M, Naldini L. Gene transfer by lentiviral vectors is limited by nuclear translocation and rescued by HIV-1 pol sequences. Nat Genet 2000;25:217–22.
35. Radulovich N, Qian JY, Tsao MS. Human pancreatic duct epithelial cell model for KRAS transformation. Methods Enzymol 2008;439:1–13.